Rare Met. (2022) 41(4):1189–1194
https://doi.org/10.1007/s12598-021-01868-0

RARE METALS

LETTER

Selective hydrogenation of 4-nitrostyrene to 4-nitroethylbenzene catalyzed by Pd@Ru core–shell nanocubes

Jing-Jing Fang, Qi-Ming Liu, Xiong-Wu Kang*, Shao-Wei Chen*

Received: 31 July 2021 / Revised: 21 August 2021 / Accepted: 2 September 2021 / Published online: 15 November 2021

It is a challenge to selectively hydrogenate 4-nitrostyrene to 4-nitroethylbenzene, due to the similar energy barrier of hydrogenation of the nitro and vinyl groups. Herein, we demonstrate that such selective hydrogenation can be achieved by Pd@Ru core–shell nanocubes that are prepared by epitaxial growth of a face-centered cubic Ru shell on Pd cubes. The core–shell structure of Pd@Ru nanocubes is confirmed by transmission electron microscopy, X-ray diffraction spectroscopy, and elemental mapping measurements. It is found that the electronic structure and hence the catalytic activity of the Pd@Ru nanocubes can be readily modulated by the Ru shell thickness. This is manifested in electrochemical CO stripping measurements where a decrease of CO adsorption energy is observed on Pd@Ru nanocubes with the increase of the Ru shell thickness. Results from this study suggest that deliberate structural engineering can be exploited to prepare bimetallic core–shell nanostructures for highly active and selective hydrogenation of organic molecules with multi-functional moieties.

Supplementary Information The online version contains supplementary material available at https://doi.org/10.1007/s12598-021-01868-0.

J.-J. Fang, X.-W. Kang*
New Energy Technology Institute, School of Environment and Energy, South China University of Technology, Guangzhou 510006, China
e-mail: esxkang@scut.edu.cn

Q.-M. Liu, S.-W. Chen*
Department of Chemistry and Biochemistry, University of California, CA 95064, USA
e-mail: shaowei@ucsc.edu

Hydrogenation of C=C double bonds is an important reaction in petrochemical, pharmaceutical, and fine chemical industries [1, 2]. Generally, molecules with a single functional group can be simply converted into the desired products by using certain metal catalysts. Yet it is challenging to achieve high selectivity in catalyzing the reaction of just one specific functional group when there exist other competing moieties in the same molecule. Hydrogenation of 4-nitrostyrene is commonly used as a model reaction since the nitro (NO_2) and vinyl (C=C) groups demonstrate a similar activation energy barrier and can both be readily hydrogenated [3–5]. In fact, the use of conventional Pt and Pd nanocatalysts can simultaneously reduce the C=C and NO_2 groups, making it difficult to achieve high selectivity for either group at high conversion efficiency. Therefore, it is of both fundamental and technological significance to develop effective, selective metal catalysts.

Controlled synthesis and engineering of metal nanomaterials has been widely demonstrated to be an effective strategy to prepare high-performance catalysts [6–8]. Palladium (Pd) and ruthenium (Ru) are two important elements of the platinum-group metals, which play critical roles in the fields of catalysis and energy transfer. In particular, Pd is known to exhibit an excellent activity and selectivity in the hydrogenation of acetylenic and olefinic moieties [9–16]. Ru-based catalysts are particularly important for many reactions, such as C–N bond formation and hydrogenation reactions. Controlled synthesis of Pd–Ru bimetallic heterostructures is an effective strategy to improve the hydrogenation performance of the catalysts [17–24]. In many reactions, Pd–Ru bimetallic alloys exhibit a better catalytic performance than their monometal counterparts, due to the manipulation of the electronic structures of Pd and Ru. For example, Huang et al. [20]

observed that alloying with Ru effectively improved Pd dispersion and modulated the electronic properties between Pd and Ru, thus enhancing the catalytic activity and selectivity of phenol hydrogenation. In another study, Li and coworkers prepared ordered porous Pd octahedra covered with a monolayer of Ru atoms, which successfully achieved semi-hydrogenation of alkynes due to the synergistic effects between the Ru monolayer and porous Pd nanocrystals [21].

Inspired by these earlier works, herein we demonstrate that the epitaxial growth of Ru layers on well-defined Pd nanocubes duplicate both the fcc crystal structure and the (100) facets of the underneath Pd nanocubes [25, 26]. Such fcc Ru layers not only inherit the high catalytic activity of Pd nanocrystals but also display much enhanced selectivity toward the hydrogenation of 4-nitrostyrene to 4-nitroethylbenzene, due to the unique surface electronic structure.

Pd@Ru core–shell nanocubes were prepared by controlled galvanic exchange reaction of Pd nanocubes with $RuCl_3$ (experimental details included in the Supporting Information) [27]. Four samples were prepared at increasing $RuCl_3$ feeds and denoted as Pd@Ru-1, Pd@Ru-2, Pd@Ru-3, and Pd@Ru-4, respectively. From TEM image in Fig. 1a, it can be seen that Pd@Ru-1 exhibits a cubic shape with an average edge length of 12.1 nm, and well-defined lattice fringes with an interplanar spacing of 0.198 nm, which can be indexed to fcc Pd and Ru (200) facets. Figure 1b, c displays a high-angle angular dark field-scanning transmission electron microscopy (HAADF-STEM) image and the corresponding line-scan profiles of Pd and Ru, which clearly show that Ru was enriched at the edges with a shell thickness about 1.72 nm (corresponding to ca. 9 atomic layers of Ru), suggesting the formation of a Pd@Ru core–shell structure. Consistent results were obtained in elemental mapping measurements based on energy-dispersive X-ray spectroscopy (EDS) (Fig. 1d). The formation of a core–shell structure in Pd@Ru-1 was further corroborated by selective acid etching of the Pd cores forming Ru nanocages (Fig. S1). The other three Pd@Ru samples also showed a cubic shape (Fig. S2); however, with an increasing $RuCl_3$ feed, the Ru shell thickness increased accordingly, ca. 2.3 nm for Pd@Ru-2, 4.7 nm for Pd@Ru-3, and 9.0 nm for Pd@Ru-4. Additionally, the nanocube surface became increasingly roughened (Pd@Ru-2 and Pd@Ru-3), and the formation of Ru islands on Pd nanocubes was even observed with Pd@Ru-4.

Further structural insights were obtained in XRD measurements. From Fig. 2, it can be seen that Pd nanocubes and Ru nanocages both exhibited four diffraction peaks at $2\theta \approx 40°$, 46°, 68°, and 82°. These can be indexed to the (111), (200), (220), and (311) facets of fcc Pd (JCPDS No. 89-4897) and fcc Ru (JCPDS No. 88-2333), indicating epitaxial growth of Ru over Pd. For the Pd@Ru-1 nanocubes, the diffraction peaks all red-shifted to a lower angle, likely because with the deposition of the Ru shell, the larger Ru atoms imposed a tensile strain on the Pd substrate (atomic radius for Ru is 0.189 versus 0.179 nm for Pd). With an increase of the Ru shell thickness, the diffraction peaks gradually shifted to a high angle and became consistent with those of Pd nanocubes and Ru nanocages, as the lattice constant of fcc Ru (a = 0.383 nm) is very close to that of fcc Pd (a = 0.389 nm) [28], allowing epitaxial growth of fcc Ru on Pd [23, 27, 29]. At an exceedingly high loading of Ru, a broad peak also emerged at around 44° for Pd@Ru-4, likely due to the (101) diffraction of hcp Ru [28]. PdRu alloy nanoparticles prepared at different atomic ratios of Pd and Ru exhibited similar XRD patterns (experimental details in Supporting Information, Fig. S3); however, the morphologies were markedly different, displaying only an irregular shape (Fig. S4).

The elemental compositions and valence states of the sample series were then examined by X-ray photoelectron spectroscopy (XPS) measurements. From Fig. 3a, it can be seen that deconvolution of the Pd 3d electrons in Pd nanocubes yielded two doublets. The first pair at 341.8 and 336.6 eV can be assigned to the $3d_{3/2}$ and $3d_{5/2}$ electrons of Pd(II), and the other one at 340.6 and 335.3 eV to Pd(0) [20, 23]. After the growth of a Ru shell on Pd, the binding energies of Pd(0) $3d_{3/2}$ and $3d_{5/2}$ increased to 341.3 and 336.0 eV, respectively, suggesting electron transfer from Pd to Ru, which became intensified with increasing Ru feed (Pd@Ru-1 to Pd@Ru-3) [23]. For Pd@Ru-4, the Ru shell was so thick that no Pd signals were observed. Similarly, two peaks can be deconvoluted in the high-resolution XPS scans of the Ru $3p_{3/2}$ electrons in Pd@Ru nanocubes at 463.7 and 461.5 eV (Fig. 3b), due to oxidized and metallic Ru, respectively [26].

For comparison, for the PdRu alloy nanoparticles (Fig. S5), only metallic Pd and Ru species were resolved, where the binding energies remained virtually invariant with the elemental composition. This suggests similar surface electronic properties among these alloy nanoparticles.

Electrochemical CO stripping measurements were then carried out to evaluate the electronic structure of the Pd@Ru nanocubes. From Figs. 4, S6 and S7, the CO oxidation peak potential (E_{CO}) of Pd@Ru, Ru-Pd alloys were derived and listed in Table 1. It can be seen that Pd nanocubes and Pd/C exhibited a voltammetric peak for CO oxidation at 0.960 and 0.919 V (vs. reversible hydrogen electrode (RHE)), respectively, and for the Pd@Ru nanocubes, the peak potential of CO oxidation was markedly reduced to 0.654 V for Pd@Ru-1, 0.612 V for Pd@Ru-2, 0.597 V for Pd@Ru-3, and 0.576 V for Pd@Ru-4 (close to that for Ru/C, 0.564 V), suggesting weakened adsorption of CO on the Pd@Ru core–shell structure and the down-shift of the d-band center by Ru deposition [30]. Notably, these peak potentials were also different from those of the

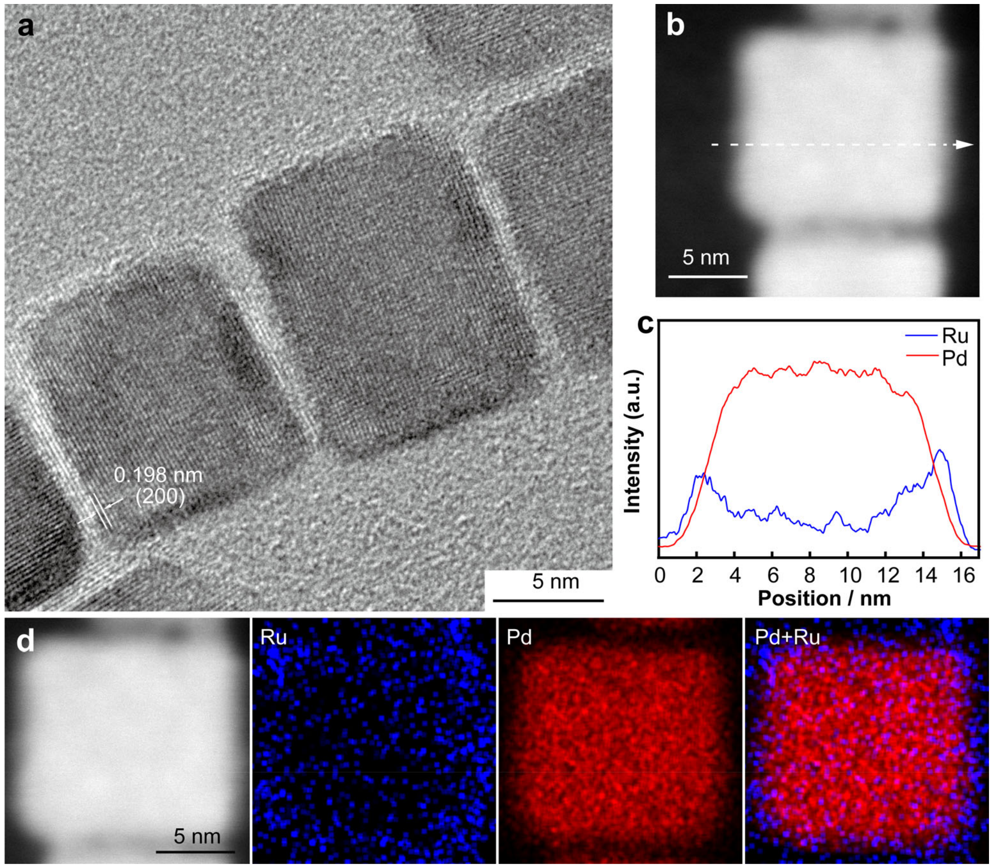

Fig. 1 **a** TEM and **b** HAADF-STEM images; **c** EDS line-scan profiles of Pd (red) and Ru (blue) along dashed arrow in panel **b**; **d** HAADF-STEM image and EDS elemental maps of Ru, Pd and Pd + Ru of Pd@Ru-1

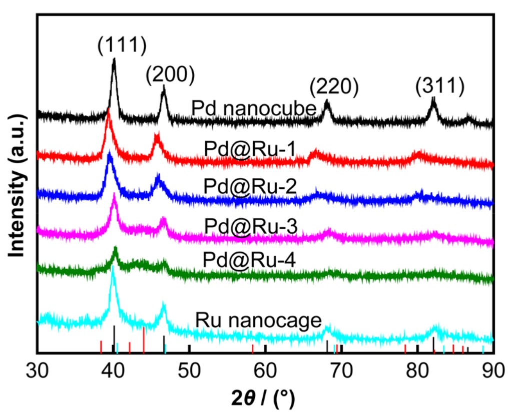

Fig. 2 XRD patterns of Pd nanocubes, Ru nanocages, and Pd@Ru nanocubes, where standard diffraction patterns of fcc Pd (black bars), hcp Ru (red bars), and fcc Ru (cyan bars) are also shown at bottom

Pd_5Ru_5 alloy nanoparticles (Fig. 4e) and somewhat higher than that of Ru nanocages (0.593 V), suggesting intimate interactions between Pd and Ru in the Pd@Ru nanocubes that modulated the surface electronic structures.

Based on the CO stripping peak areas, the electrochemical active surface area (ECSA) was then evaluated [28], and the results are summarized in Table 1. It can be seen that with the growth of a Ru shell, the ECSA increased substantially, consistent with the increasing roughness of the nanocube morphology, as observed in TEM measurements (Figs. 1, S2).

The catalytic activity and selectivity of the Pd@Ru nanocubes toward the hydrogenation of 4-nitrostyrene to 4-nitroethylbenzene and 4-ethylbenzenamine was then evaluated and compared. From Fig. 5, it can be seen that all Pd@Ru nanocubes exhibited 100% selectivity in the hydrogenation of 4-nitrostyrene to 4-nitroethylbenzene, with no detectable production of 4-ethylbenzeneamine. Yet the activity varied among the samples. Specifically, From Fig. 5a, Pd@Ru-1 nanocubes can be seen to exhibit the best performance among the sample series, achieving 100% conversion of 4-nitrostyrene to 4-nitroethylbenzene in 60 min and maintaining the 100% efficiency thereafter. Pd@Ru-2 exhibited a somewhat lower catalytic activity (Fig. 5b), with 100% production of 4-nitroethylbenzene in 3 h. The catalytic activity was even lower with Pd@Ru-3 and Pd@Ru-4, suggesting that a thick Ru shell and reduced adsorption energy is not favorable for the selective hydrogenation of the nitro group (Table 1) [31].

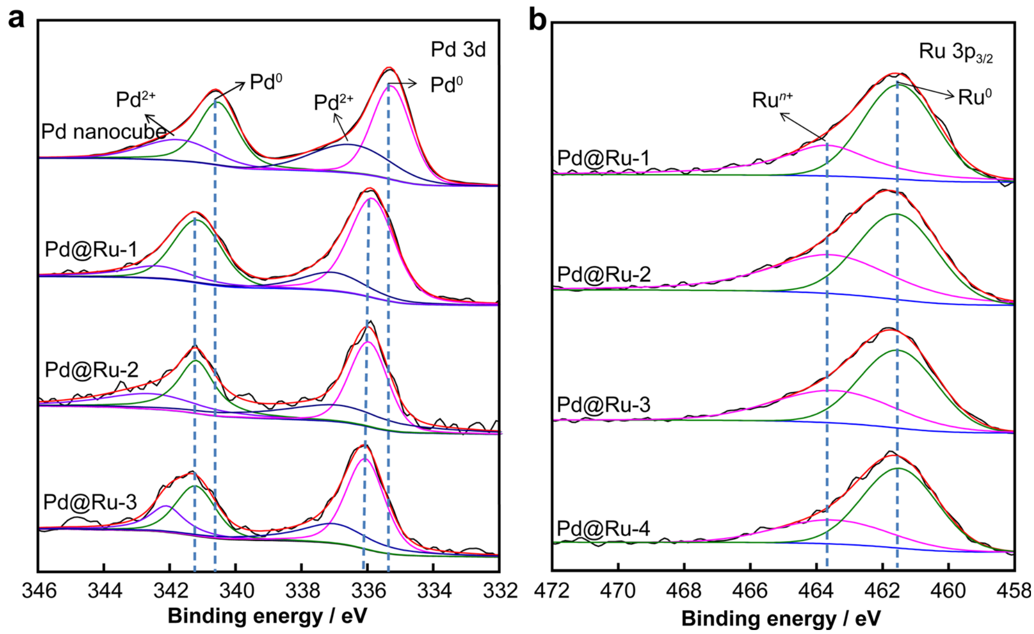

Fig. 3 High-resolution XPS spectra of **a** Pd 3d and **b** Ru 3p$_{3/2}$ electrons in Pd and Pd@Ru nanocubes. Black curves are experimental data and colored curves are deconvolution fits

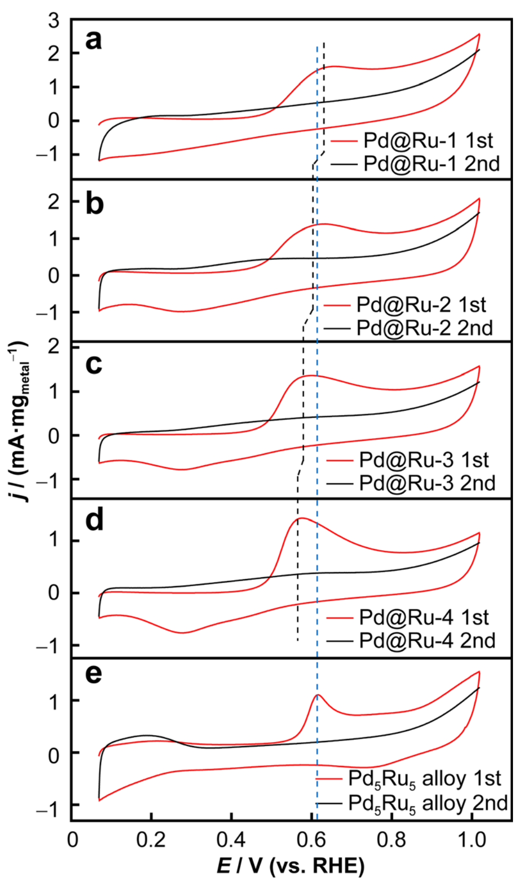

Fig. 4 First and second scans of the CO stripping voltammograms of **a** Pd@Ru-1, **b** Pd@Ru-2, **c** Pd@Ru-3, **d** Pd@Ru-4, and **e** Pd$_5$Ru$_5$ alloys in 0.5 mol·L^{-1} H_2SO_4 at the potential scan rate of 50 mV·s^{-1}

Table 1 CO oxidation peak potentials (E_{CO}) and electrochemical active surface areas (ECSA) of the sample series

Sample	E_{CO} /V	ECSA/(m^2.g^{-1})
Pd nanocubes	0.960	0.10
Pd@Ru-1	0.654	48.10
Pd@Ru-2	0.612	61.70
Pd@Ru-3	0.597	79.70
Pd@Ru-4	0.576	88.20
Pd/C	0.919	36.10
Ru nanocages	0.593	65.10
Ru/C	0.564	1.41
Pd_3Ru_7	0.601	29.90
Pd_5Ru_5	0.616	31.70

For comparison, Pd nanocubes (Fig. S8a), Pd/C (Fig. S8b) and PdRu alloy nanoparticles (Fig. S8c–e) exhibited markedly different catalytic performances. It can be seen that at the initial stage, 4-nitroethylbenzene was the primary product of hydrogeneration, whereas at prolonged reaction times, 4-ethylbenzeneamine became the increasingly dominant species. By sharp contrast, Ru/C (Fig. S8f) and fcc Ru nanocages (Fig. S8g) exhibited virtually no catalytic activity. These observations suggest that the surface Pd species, rather than the Ru ones, were the catalytic active sites responsible for the hydrogenation of 4-nitrostyrene to 4-ethylbenzeneamine, where the reaction mechanism entailed sequential hydrogenation of the vinyl and nitro groups in 4-nitrostyrene [17–24]. From Table 1, it can be seen that the ECSA of Pd@Ru-1 is the lowest

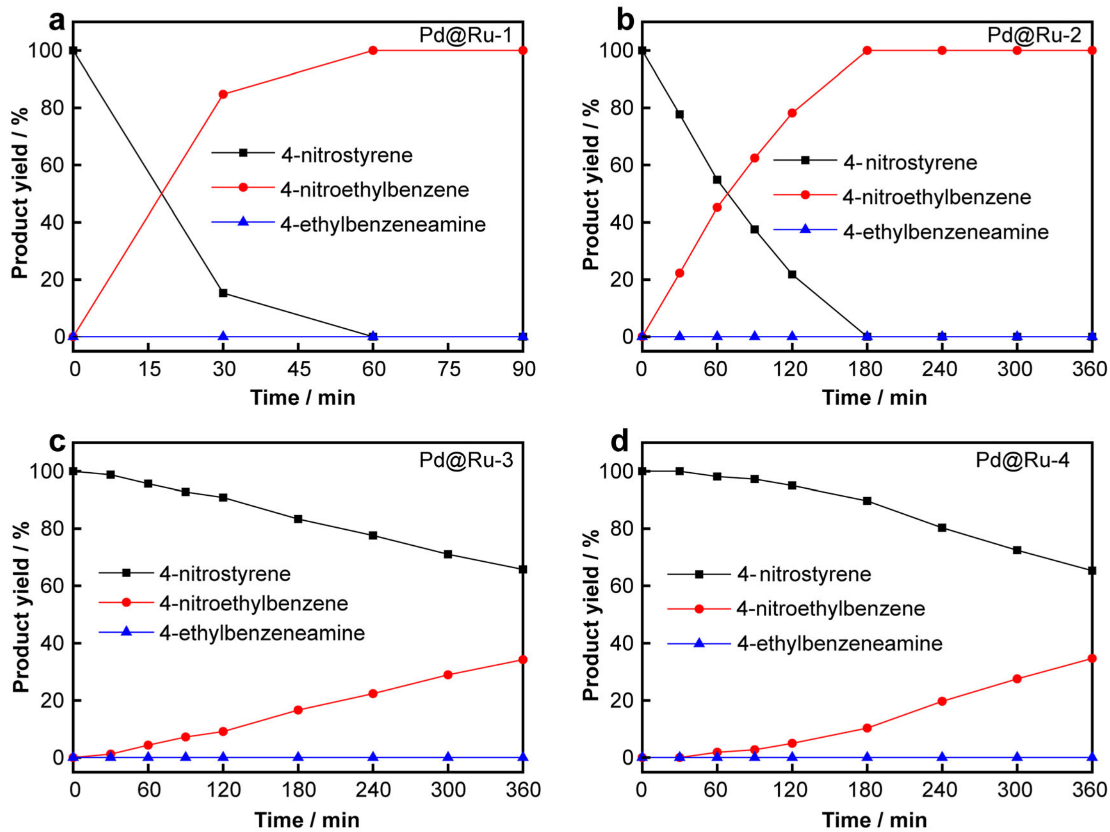

Fig. 5 Hydrogenation products of 4-nitrostyrene catalyzed by **a** Pd@Ru-1, **b** Pd@Ru-2, **c** Pd@Ru-3, and **d** Pd@Ru-4

among the four Pd@Ru samples, yet the activity was the best. This suggests that surface morphology (and surface area) did not play a significant role in the determination of the catalytic performance. Rather, it is the surface electronic structure that dictates the hydrogenation activity.

Notably, Pd@Ru-1 and Pd@Ru-2 also exhibited good stability (Fig. S9a, b), where the catalytic activity and selectivity remained virtually invariant in repeated tests. This performance is obviously better than those of Pd nanocubes, Pd/C, Pd_5Ru_5, and Pd_3Ru_7 (Fig. S9c–f), signifying the unique advantage of the core@shell morphology in the catalytic reaction.

The fact that the Pd@Ru core@shell nanocubes exhibited 100% selective production of 4-nitroethylbenzene from the hydrogenation of 4-nitrostyerene suggests that the subsequent reduction of the nitro group was impeded, most likely due to the limited number of Pd sites on the nanocube surface (Figs. 1, S2) that became electron-deficient as a result of charge transfer to Ru, as manifested in XPS measurements (Fig. 3), in comparison to those of Pd nanocubes, Pd/C, and PdRu alloy nanoparticles (Fig. S5). This resulted in a weakened Pd–Pd metallic bond in Pd@Ru and hence preferential adsorption and hydrogenation of the functional moiety of lower polarity, i.e., the vinyl group in 4-nitrostyerene, over the more polar (nitro) group [5]. Taken together, these results suggest that the synergistic interaction between Pd and Ru in Pd@Ru core–shell nanocubes can be exploited for the effective manipulation of the surface electronic property and ultimately selective hydrogenation of 4-nitrostyrene to 4-nitroethylbenzene.

In summary, the hydrogenation dynamics of 4-nitrostyrene on Pd nanocubes were readily modulated by epitaxial growth of an fcc Ru shell, achieving high selectivity toward the production of 4-nitroethylbenzene. In contrast, no catalytic activity was observed with commercial Ru and fcc Ru nanocages, and only poor selectivity with Pd nanocubes, commercial Pd and PdRu alloys. Electrochemical CO stripping studies demonstrated a reduced adsorption energy of the reactants on fcc Ru-modified Pd, and the unique core–shell structure accounted for the selective hydrogenation of the vinyl group in 4-nitrostyrene, whereas the subsequent hydrogenation of the nitro moiety was impeded with the electron-deficient Pd sites. Results from this study suggest that deliberate alloying may be exploited as an effective strategy to manipulate the electronic structure of the catalyst surface for enhanced catalytic activity and selectivity in the hydrogenation of organic molecules.

Acknowledgements This study was financially supported by the Fundamental Research Funds for Central Universities (No. 2019ZD22) and Guangdong Innovative and Entrepreneurial Research Team

Program (No. 2016ZT06N569). S. W. Chen thanks the National Science Foundation for partial support of the work (No. CHE-2003685).

Declarations

Conflict of interests The authors declare that they have no conflict of interest.

References

[1] Mao J, Chen W, Sun W, Chen Z, Pei J, He D, Lv C, Wang D, Li Y. Rational control of the selectivity of a ruthenium catalyst for hydrogenation of 4-nitrostyrene by strain regulation. Angew Chem Int Ed Engl. 2017;56(39):11971.

[2] Zhang W, Wu W, Long Y, Qin JH, Wang FS, Ma JT. Promoting role of iron series elements modification on palladium/nitrogen doped carbon for the semihydrogenation of phenylacetylene. ChemCatChem. 2019;11(5):1510.

[3] Xu G, Wei H, Ren Y, Yin J, Wang A, Zhang T. Chemoselective hydrogenation of 3-nitrostyrene over a Pt/FeO_x pseudo-single-atom-catalyst in CO_2-expanded liquids. Green Chem. 2016;18(5):1332.

[4] Corma A, Serna P. Chemoselective hydrogenation of nitro compounds with supported gold catalysts. Science. 2006;313(5785):332.

[5] Yang N, Cheng H, Liu X, Yun Q, Chen Y, Li B, Chen B, Zhang Z, Chen X, Lu Q, Huang J, Huang Y, Zong Y, Yang Y, Gu L, Zhang H. Amorphous/crystalline hetero-phase Pd nanosheets: one-pot synthesis and highly selective hydrogenation reaction. Adv Mater. 2018;30(39):1803234.

[6] Pei YC, Qi ZY, Goh TW, Wang LL, Maligal-Ganesh RV, MacMurdo HL, Zhang SR, Xiao CX, Li XL, Tao F, Johnson DD, Huang WY. Intermetallic structures with atomic precision for selective hydrogenation of nitroarenes. J Catal. 2017;356:307.

[7] Maligal-Ganesh RV, Xiao CX, Goh TW, Wang LL, Gustafson J, Pei YC, Qi ZY, Johnson DD, Zhang SR, Tao F, Huang WY. A ship-in-a-bottle strategy to synthesize encapsulated intermetallic nanoparticle catalysts: exemplified for furfural hydrogenation. Acs Catal. 2016;6(3):1754.

[8] Yang YL, Xie YF, Zhang J, Li DM, Deng DS, Duan Y. Fabrication of Pd/SiO_2 with controllable wettability for enhanced catalytic hydrogenation activity at ambient H_2 pressure. ChemCatChem. 2019;11(22):5430.

[9] Liu H, Jiang T, Han B, Liang S, Zhou Y. Selective phenol hydrogenation to cyclohexanone over a dual supported Pd–lewis acid catalyst. Science. 2009;326(5957):1250.

[10] Huang F, Deng Y, Chen Y, Cai X, Peng M, Jia Z, Ren P, Xiao D, Wen X, Wang N, Liu H, Ma D. Atomically dispersed Pd on nanodiamond/graphene hybrid for selective hydrogenation of acetylene. J Am Chem Soc. 2018;140(41):13142.

[11] Wang Y, Yao J, Li H, Su D, Antonietti M. Highly selective hydrogenation of phenol and derivatives over a Pd@carbon nitride catalyst in aqueous media. J Am Chem Soc. 2011;133(8):2362.

[12] Ma X, Jiang T, Han B, Zhang J, Miao S, Ding K, An G, Xie Y, Zhou Y, Zhu A. Palladium nanoparticles in polyethylene glycols: efficient and recyclable catalyst system for hydrogenation of olefins. Catal Commun. 2008;9(1):70.

[13] Zhang Q, Li J, Liu X, Zhu Q. Synergetic effect of Pd and Ag dispersed on Al_2O_3 in the selective hydrogenation of acetylene. Appl Catal A. 2000;197(2):221.

[14] Studt F, Abild-Pedersen F, Bligaard T, Sorensen RZ, Christensen CH, Norskov JK. On the role of surface modifications of palladium catalysts in the selective hydrogenation of acetylene. Angew Chem Int Ed Engl. 2008;47(48):9299.

[15] Jørgensen M, Grönbeck H. Selective acetylene hydrogenation over single-atom alloy nanoparticles by kinetic monte carlo. J Am Chem Soc. 2019;141(21):8541.

[16] Chen Z, Wang W, Zhang Y, Liang Y, Cui Z, Wang X. Pd nanoparticles confined in the porous graphene-like carbon nanosheets for olefin hydrogenation. Langmuir. 2018;34(43):12809.

[17] Wu D, Kusada K, Kitagawa H. Recent progress in the structure control of Pd–Ru bimetallic nanomaterials. Sci Technol Adv Mater. 2016;17(1):583.

[18] Ye H, Wang Q, Catalano M, Lu N, Vermeylen J, Kim MJ, Liu Y, Sun Y, Xia X. Ru nanoframes with an fcc structure and enhanced catalytic properties. Nano Lett. 2016;16(4):2812.

[19] Kusada K, Kobayashi H, Ikeda R, Kubota Y, Takata M, Toh S, Yamamoto T, Matsumura S, Sumi N, Sato K, Nagaoka K, Kitagawa H. Solid solution alloy nanoparticles of immiscible Pd and Ru elements neighboring on Rh: changeover of the thermodynamic behavior for hydrogen storage and enhanced CO-oxidizing ability. J Am Chem Soc. 2014;136(5):1864.

[20] Huang C, Yang X, Yang H, Huang P, Song H, Liao S. High-performance PdRu bimetallic catalyst supported on mesoporous silica nanoparticles for phenol hydrogenation. Appl Surf Sci. 2014;315:138.

[21] Ge J, He D, Bai L, You R, Lu H, Lin Y, Tan C, Kang YB, Xiao B, Wu Y, Deng Z, Huang W, Zhang H, Hong X, Li Y. Ordered porous Pd octahedra covered with monolayer Ru atoms. J Am Chem Soc. 2015;137(46):14566.

[22] Furukawa S, Yoshida Y, Komatsu T. Chemoselective hydrogenation of nitrostyrene to aminostyrene over Pd- and Rh-based intermetallic compounds. ACS Catal. 2014;4(5):1441.

[23] Zhang Z, Liu Y, Chen B, Gong Y, Gu L, Fan Z, Yang N, Lai Z, Chen Y, Wang J, Huang Y, Sindoro M, Niu W, Li B, Zong Y, Yang Y, Huang X, Huo F, Huang W, Zhang H. Submonolayered Ru deposited on ultrathin Pd nanosheets used for enhanced catalytic applications. Adv Mater. 2016;28(46):10282.

[24] Corma A, Serna P, Concepcion P, Calvino JJ. Transforming nonselective into chemoselective metal catalysts for the hydrogenation of substituted nitroaromatics. J Am Chem Soc. 2008;130(27):8748.

[25] Fan Z, Zhang H. Template synthesis of noble metal nanocrystals with unusual crystal structures and their catalytic applications. Acc Chem Res. 2016;49(12):2841.

[26] Zhao M, Chen Z, Lyu Z, Hood ZD, Xie M, Vara M, Chi M, Xia Y. Ru octahedral nanocrystals with a face-centered cubic structure, 111 facets, thermal stability up to 400 degrees C, and enhanced catalytic activity. J Am Chem Soc. 2019;141(17):7028.

[27] Zhao M, Figueroa-Cosme L, Elnabawy AO, Vara M, Yang X, Roling LT, Chi M, Mavrikakis M, Xia Y. Synthesis and characterization of Ru cubic nanocages with a face-centered cubic structure by templating with Pd nanocubes. Nano Lett. 2016;16(8):5310.

[28] Gu J, Guo Y, Jiang YY, Zhu W, Xu YS, Zhao ZQ, Liu JX, Li WX, Jin CH, Yan CH, Zhang YW. Robust phase control through hetero-seeded epitaxial growth for face-centered cubic Pt@Ru nanotetrahedrons with superior hydrogen electro-oxidation activity. J Phys Chem C. 2015;119(31):17697.

[29] Alayoglu S, Nilekar AU, Mavrikakis M, Eichhorn B. Ru-Pt core-shell nanoparticles for preferential oxidation of carbon monoxide in hydrogen. Nat Mater. 2008;7(4):333.

[30] Guo Z, Kang X, Zheng X, Huang J, Chen S. PdCu alloy nanoparticles supported on CeO_2 nanorods: enhanced electrocatalytic activity by synergy of compressive strain, PdO and oxygen vacancy. J Catal. 2019;374:101.

[31] Zhang S, Chang CR, Huang ZQ, Li J, Wu Z, Ma Y, Zhang Z, Wang Y, Qu Y. High catalytic activity and chemoselectivity of sub-nanometric Pd clusters on porous nanorods of CeO_2 for hydrogenation of nitroarenes. J Am Chem Soc. 2016;138(8):2629.